# Chapter 4

# Results and discussions

This chapter will present the experimental results based on hydrothermal method, which is preferential compared to other techniques. The hydrothermal method was employed to synthesize vertically aligned $TiO_2$ NRs on FTO substrate assisted by $TiO_2$ seed layer. As shown in chapter 3, three interesting parameters in preparation of vertically aligned $TiO_2$ NRs were considered consisting of calcination temperature, precursor concentration and reaction time. Finally, the synthesis products were characterized by field emission scanning electron microscopy ( FE-SEM) , x-ray diffraction (XRD), UV-vis spectroscopy, and transmission electron microscope (TEM).

## 4.1 Effect of seed layer

### 4.1.1 Characterization of morphology by field emission scanning electron microscopy (FE-SEM)

In this work, FTO-coated glass with 562 nm thickness was used as substrate. Uniformly distributed $TiO_2$ seed layers ( SLs) were coated on the FTO substrate consisting of nanoparticles with a mean diameter and thickness of 27 nm and 101 nm, respectively. Figure 4.1 (a-b) shows the FE-SEM images of the FTO surface and $TiO_2$ SLs surface. It revealed that the roughness on FTO surface was superior compared to that on the SLs surface. This could result in $TiO_2$ NRs grown on the bare FTO showing terrible vertical orientation that some NRs almost collapsed and paralleled to the horizontal direction. The neighboring NRs collided with each other that could prevent the electron transfer (Figure 4.1 (c,e)). On the other hands, SLs provide a lower surface roughness thereby oriented NRs arrays were obtained significantly. This led to an increase in density and vertical orientation of the NRs, which is expected to achieve a high electron transport as shown in ( Figure 4. 1 ( b,d) ) . The results of the study correspond with James E.S. Haggerty et al, showing that the seeded-FTO films with smaller roughness would benefit to grow denser nanorods [36]. Average diameter of the $TiO_2$ NRs on FTO was 41 nm and that on SLs was 78 nm. This represents that dimensions of the $TiO_2$ NRs grown on SLs are larger than those grown on bare FTO. This can be attributed to smooth surface of SLs promote nucleation of rutile

$TiO_2$ leading to high vertical alignment of NRs. This contributes to development of NRs in height and in width**.** From nergy-dispersive ıl-ray spectroscopy (EDS) analysis, the atomic ratio of Ti to O is nearly 1 : 2.

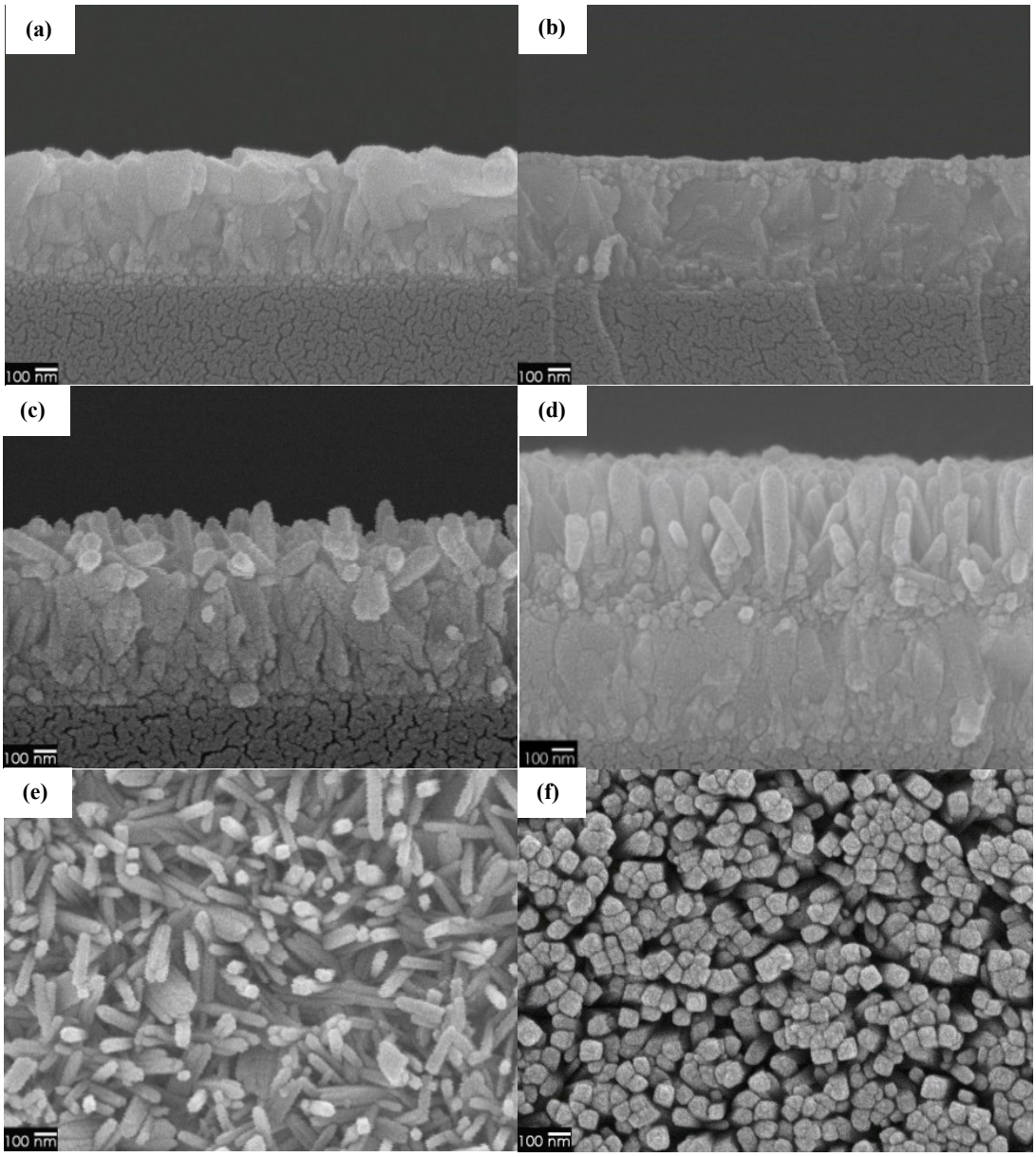


**Figure 4.1** Cross section FE-SEM images of (a) FTO (b) seed on FTO (c) 1.0% $TiO_2$ NRs on FTO (d) 1.0% $TiO_2$ NRs on seed layers. (e) Top view FE-SEM images of 1.0% TBO NRs on FTO (f) Top view FE-SEM images 1.0% TBO NRs on seed layers

### 4.1.2 Characterization of crystallinity by X-ray diffraction (XRD)

Figure 4.2 (a) shows that all diffraction peaks of SLs agree well with the dominate (001) anatase tetragonal plane with small a (200) peak. Even though SLs were anatase structure, the characteristic peaks of 1.0% TBO NRs on SLs demonstrate (101) and (002) rutile (Figure 4.3 (a)). Because the hydrothermal procedure was conducted in hydrochloric acid (HCl) diluted with deionized water (DI) and Ti(IV)-butoxide (TBO) was applied as a reactant with structure formula. When the four-fold Ti precursor ($[Ti(RO)_4]$) reacts with water, the coordination number of $Ti^{4+}$ increases from four to six to accept oxygen lone pairs forming Ti-O bond. During the particle agglomeration, the acidity of the reaction solution is suggested as a critical factor. $H_2O$ participates in hydrolysis by separating butoxy groups [OR] from Ti atoms and replacing with dissociated hydroxyl groups [$OH^-$] in the solution. In addition, HCl takes responsible to protonate OH− in Ti-hydroxo [22]. By the attribution of dehydration (elimination of water molecules), Ti-hydroxo could be combined into the precipitate crystal.

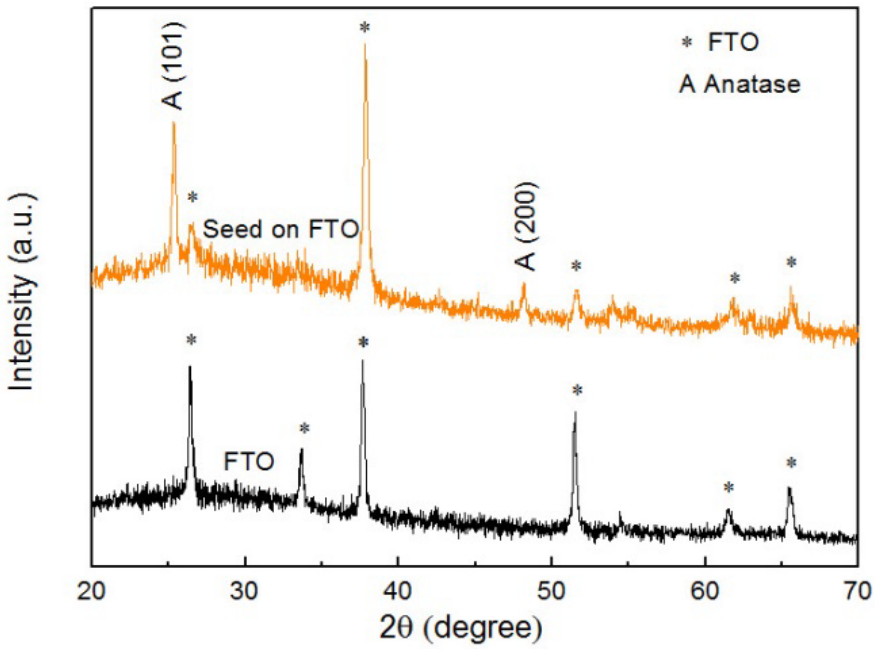


**Figure 4.2** XRD patterns of bare FTO and $TiO_2$ seed layers on FTO.

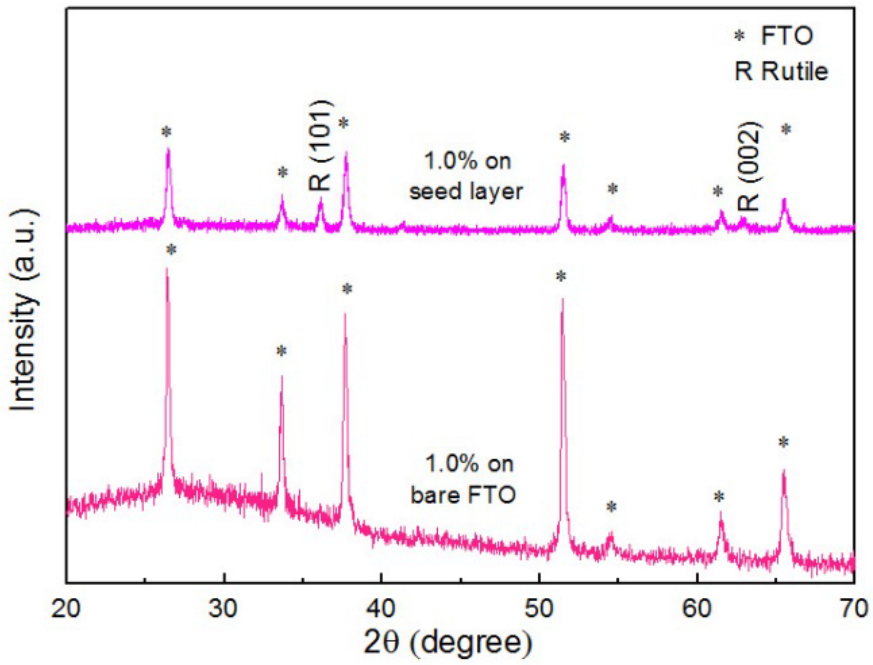


**Figure 4.3** XRD patterns of 1.0% TBO $TiO_2$ NRs on bare FTO and $TiO_2$ NRs on seed/FTO by hydrothermal reaction at 150°C for 1.5 h

Recently, the similar hydrothermal approach with the resembling hydrothermal solution using TBO, HCl and DI water, reported the XPS data supporting that present of maximum oxygen in $TiO_2$ which comes from OH and $OH_2$ groups. In addition, the surface hydroxide ions contribute to the 1D growth of single crystalline $TiO_2$ nanorods on FTO substrate [33]. The anatase and rutile phases are the results from nanorods synthesis on seed layer by hydrothermal method using pH 4-5 and pH 1-2 synthesis solutions, respectively [19]. Since rutile phase requires high degree protonation of $TiO_6$ octahedra to form their favourable dense orientation that means it desires advanced acid intensity to effectively catalyse the hydrolysis and dehydration reaction [21]. Moreover, characteristic anatase architecture is not stable under highly acidic conditions because of strong repulsion between the protonated molecules within crystal structure [21]. Therefore, only rutile $TiO_2$ NRs can be nucleated in acid medium. In the present work, the 1-2 pH hydrothermal solution was used which had strong acidity for crystal formation into rutile.

Previous study reported that the dominate crystal plane of NRs in length of 1-2 μm on seed layers was (002) and (101) for NRs on FTO. This indicated that seed layers provided the nucleation of the higher surface energy (002) plane of tetragonal rutile $TiO_2$ NRs [19, 21]. However, here the characteristic patterns of NRs on FTO were not

able to observe (Figure 4.3) because the density of the NRs was too low to detect by XRD machine. However, FTO substrate FTO was produced from occupation of F in O position in $SnO_2$ structure which is rutile tetragonal lattice with the same phase as $TiO_2$ rutile (confirmed by ICDD database code number 00-001-0625). In addition, XRD peaks of FTO exhibit the rutile $SnO_2$ pattern. The lattice mismatch between the tetragonal $SnO_2$ ($a = b = 0.4687$ nm) and the anatase $TiO_2$ ($a = b = 0.4594$ nm) is only 2%. Hence, bare FTO substrate could promote the epitaxial nucleation and growth orientation of the rutile $TiO_2$ nanorods. Moreover, the hydrothermal medium was conducted in high acidity solution, and then it can be assumed that NRs grown on FTO had $TiO_2$ rutile structure.

## 4.2 Effect of calcination at high temperature

### 4.2.1 Characterization of morphology by field emission scanning electron (FE-SEM)

From Figure 4.4 (a-b), calcined 0.7% TBO $TiO_2$ NRs at 500ºC show the larger length (270 nm) than that of non calcined 0.7% $TiO_2$ NRs (196 nm). Similar to diameter, calcined 0.7% and non calcined NRs displayed 51 nm and 45 nm in diameter, respectively as shown in Figure 4.4 (c-d). This indicates that calcination is attributed to enlarge the height and diameter of calcined 0.7% TBO NRs. Similary, calcined 1.0% TBO NRs had diameter greater (78 nm) than that of pre-calcination or non calcined NRs (67 nm). It can be assumed that the thermal energy from calcination could be converted into binding energy between Ti-O beccause some Ti-complexes from hydrothermal process still have oxigen vacancies. The calcination at high temperature could contribute to produce the complete $TiO_2$ then crystallinity of $TiO_2$ was higher and this could elongate the length and diameter of NRs.

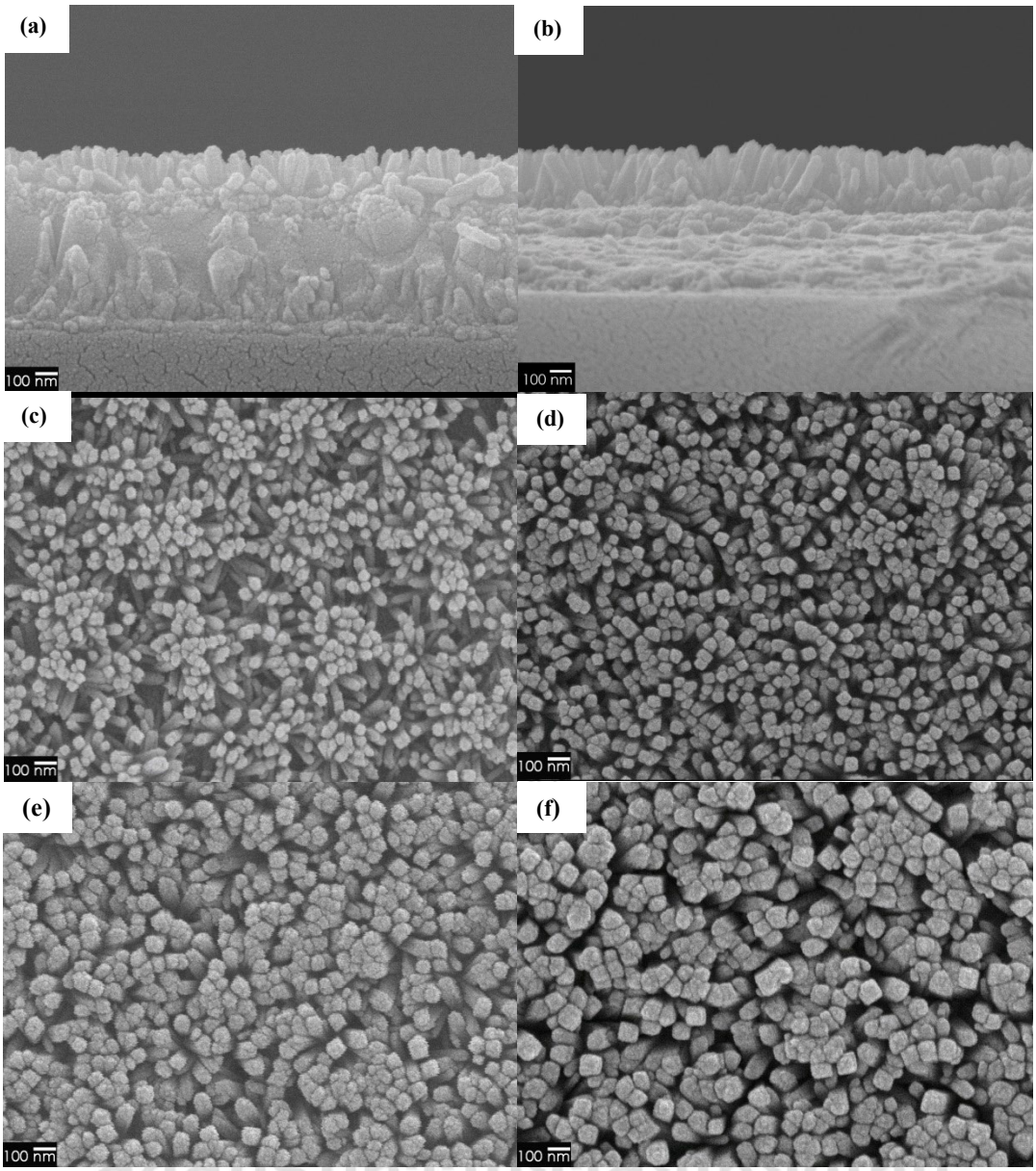


**Figure 4.4** Cross section FE-SEM images of (a) non calcined 0.7% TBO $TiO_2$ NRs (b) calcined 0.7% TBO $TiO_2$ NRs, Top view FE-SEM images of (c) non calcined 0.7% TBO NRs (d) calcined 0.7% TBO NRs (e) non calcined 1.0 % TBO NRs (f) calcined 1.0% TBO NRs

### 4.2.2 Characterization of crystallinity by X-ray diffraction (XRD)

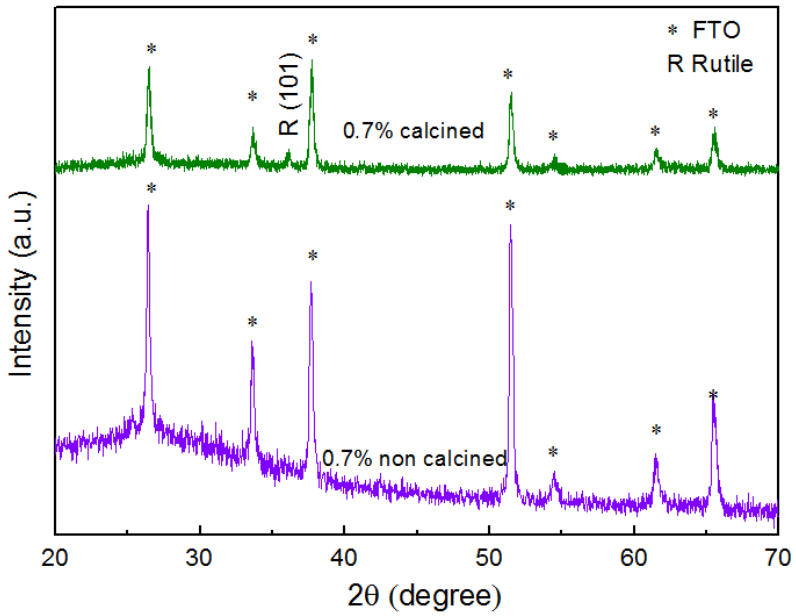


**Figure 4.5** XRD patterns of 0.7% TBO $TiO_2$ NRs showing non calcined and calcined

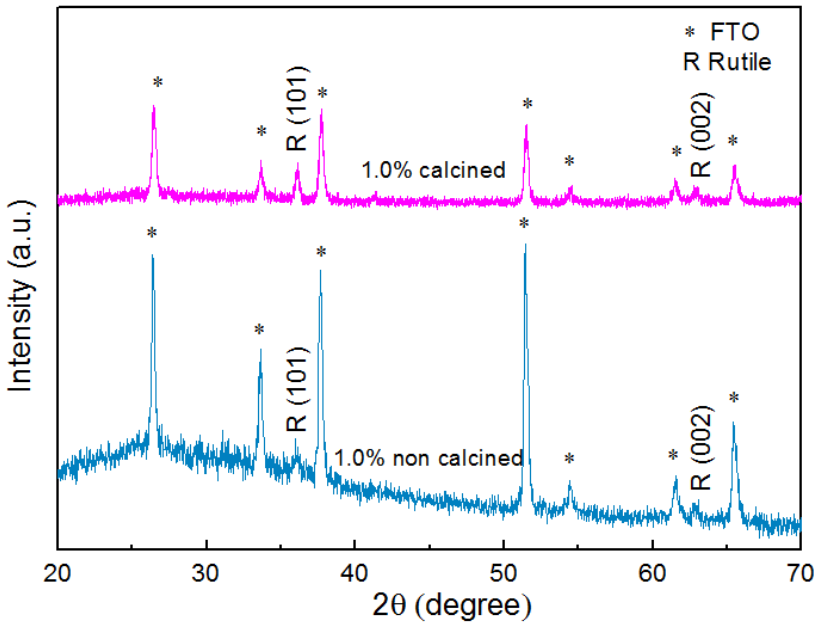


**Figure 4.6** XRD patterns of 0.7% TBO $TiO_2$ NRs including non calcined and calcined

Corresponding with SEM results, non-calcined 0.7 $TiO_2$ NRs (0.7 nc-NRs) show (101) rutile $TiO_2$ peak while none of characteristic peak of $TiO_2$ could be observed in calcined 0.7% $TiO_2$ NRs (0.7 c-NRs) as shown in Figure 4.5. Figure 4.6 illustrates that calcined 1.0 % TBO NRs had intensity of (101) rutile and (002) rutile phase higher than calcined 1. 0% TBO NRs. The evidences support that calcination could improve construction of crystallinity. Because at high temperature, the particle size in hydrothermal calcination should be larger after the transformation if the crystallization occurs with further atoms [38].

### 4.3 Effect of precursor concentration

#### 4.3.1 Characterization of morphology by field emission scanning electron (FE-SEM)

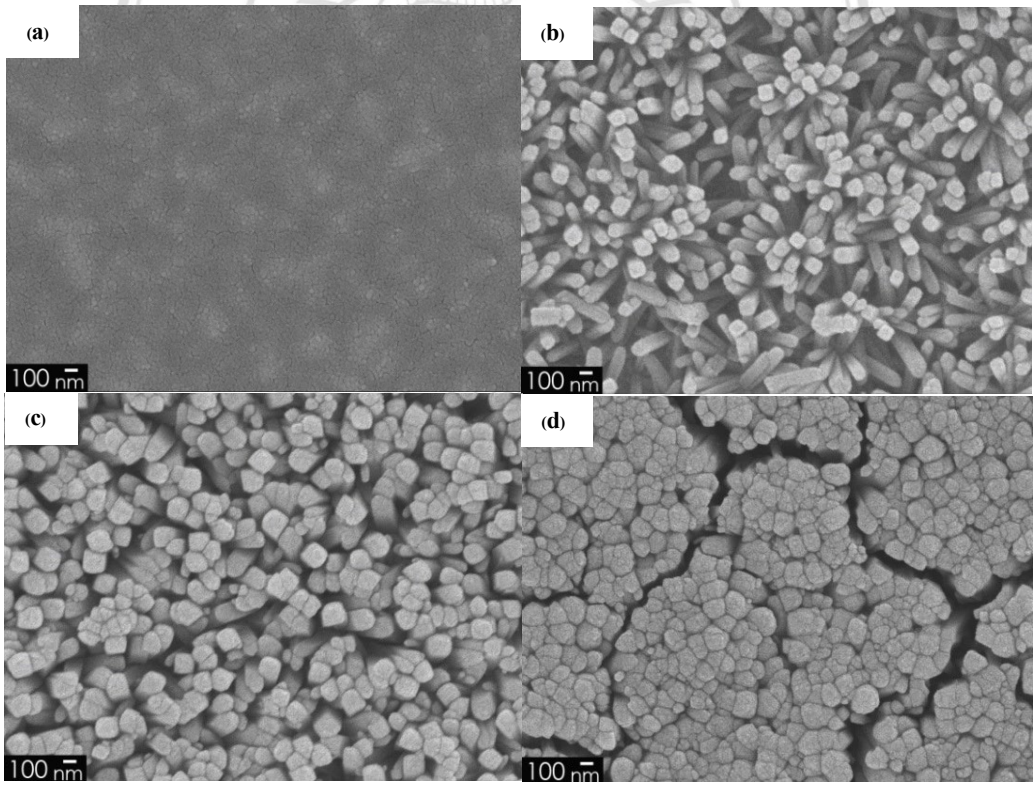


**Figure 4.7** Top view FE-SEM images of $TiO_2$ nanorods using titanium IV butoxide (TBO) (a) 0.1%, (b) 0.5 %, (c) 1.0%, and (d) 1.5%

If TBO concentration is not sufficient to begin nucleation of NRs, even though the hydrothermal was conducted for 2h, the NRs could not be successfully formed (Figure 4.7 (a), (0.1% TBO)). In case of too high concentration of TBO such as 1.5%,

the coagulation of NRs can observe and the chasms took place on the film surface resulting in non homogeneous film surface. In order to reduce surface roughness, seed layers that compose of $TiO_2$ play significant role. Growth of $TiO_2$ NRs by hydrothermal method, the seed layers provide a smooth surface compared to FTO surface thereby oriented NRs arrays were obtained [19]. Due to $TiO_2$ compact as seed layers and FTO as substrates, in case of having sufficient precursors as 0.7% and 1.0% TBO, the vertically well-aligned NRs are expected.

The surface morphology of $TiO_2$ NRs was observed by FE-SEM as exhibited in Figure 4.8. This Figure shows the cross-sectional images and top view of $TiO_2$ NRs hydrothermally grown on $TiO_2$ seed layers prepared on FTO substrates for 1.5 h. As seen in Figure 4.8 (b), the growth distribution of $TiO_2$ NRs using 0.3% TBO precursor showed initial nucleation randomly scattered over $TiO_2$ surface. While the TBO concentration increased to 0.5% (Figure 4.7 (d)), there were still discontinuous patterns of tiny NRs with small diameter very close to those in 0.3% TBO, but the length was 3 times longer (Figure 4.8 (c)). The well-distributed $TiO_2$ NRs vertically aligned and covered entire seed surface observed in 0.7% TBO concentration. Noticeably, $TiO_2$ NRs at 1.0% TBO densely packed and completely oriented normal to the substrate, as shown in Figure 4.8 (g, h).

**Table 4.1** Average diameter and length of $TiO_2$ NRs at various TBO concentrations

| Concentration of TBO (%) | Diameter (*nm*) | Length (*nm*) |
|---|---|---|
| 0.3 | 31 | 28 |
| 0.5 | 34 | 103 |
| 0.7 | 51 | 270 |
| 1.0 | 78 | 522 |

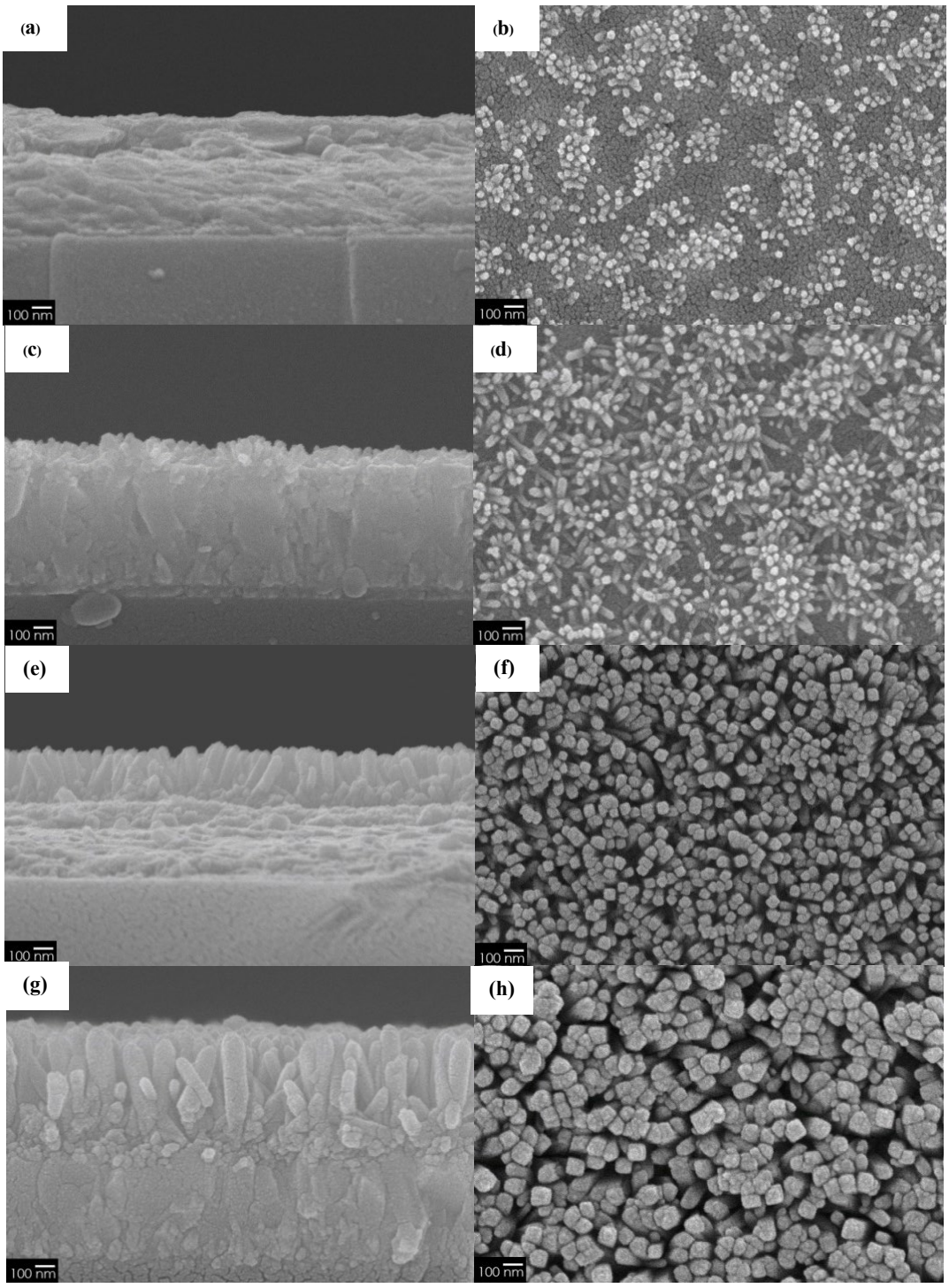


**Figure 4.8** Cross-section view and top view FE-SEM images of $TiO_2$ nanorods using titanium IV butoxide (TBO) (a,b) 0.3%, (c,d) 0.5% (e, f) 0.7%, and (g,h) 1.0 %

From FE-SEM images, the average diameter and length can be approximated by using ImageJ software, as displayed in Table 4.1. The results showed that an increase in the TBO concentration favored a simultaneous increase in average diameter and length of $TiO_2$ NRs. This indicates that low percentage of TBO ($<0.5\%$) is not enough to construct well-align $TiO_2$ NRs, leading to misoriented NRs. Therefore, the arrangement of $TiO_2$ NRs is not vertically ordered and does not cover entire substrate surface. The increment of TBO precursor leads to prompt hydrolysis and precipitation reaction of the growth solution on seeded FTO surface [4]. A great number of nucleation sites on the substrate surface is a result of a large amount of the precursor in high TBO concentration. In the same processing time, dimensions of higher percentage TBO NRs are larger because of rapid growth reaction and large region of initial nucleation sites. Proportion of diameter and length of $TiO_2$ NRs was improved with increasing of TBO concentration, corresponding to the works by Kim H. et al. [19] and Liu B. et al. [4].

### 4.3.2 Characterization of crystallinity by X-ray diffraction (XRD)

Figure 4.9 exhibits the XRD patterns of $TiO_2$ NRs (0.3%-1.0% TBO) toghter with $TiO_2$ seed layer prepared on a FTO (seed/FTO) with 2θ range of 20-70 degrees. (Owning to small length of $TiO_2$ NRs compared to FTO thickness (580 nm), the intensity of FTO patterns were dramatically present.) The results show that a diffraction peak agrees well with $TiO_2$ tetragonal rutile structure ICDD No. 00-002-0494 (with lattice parameter $a = b = 4.58$ Å and $c = 2.950$ Å, P42/mnm SG). A dominant $TiO_2$ tetragonal rutile peak corresponds to **(**101**)** reflection**.** This rutile phase clearly emerged if TBO reactant increased up to 0.7%. Additionally, 1.0 % the TBO concentration there was a small amount of rutile (002) plane as well (according to ICDD No.00-002-0494). From preliminary results in very high TBO concentration (>1.0 %), rutile (002) peak is dominate with high density indicating that high crystallinity NRs compose of (002) plane as majority plane. Because **(**101**)** is one of the lowest surface energy plane of rutile $TiO_2$, they require lower energy to form crystal along this plane [20]. When TBO percentage approaches to 1.0%, formations of rutile (002) occur.

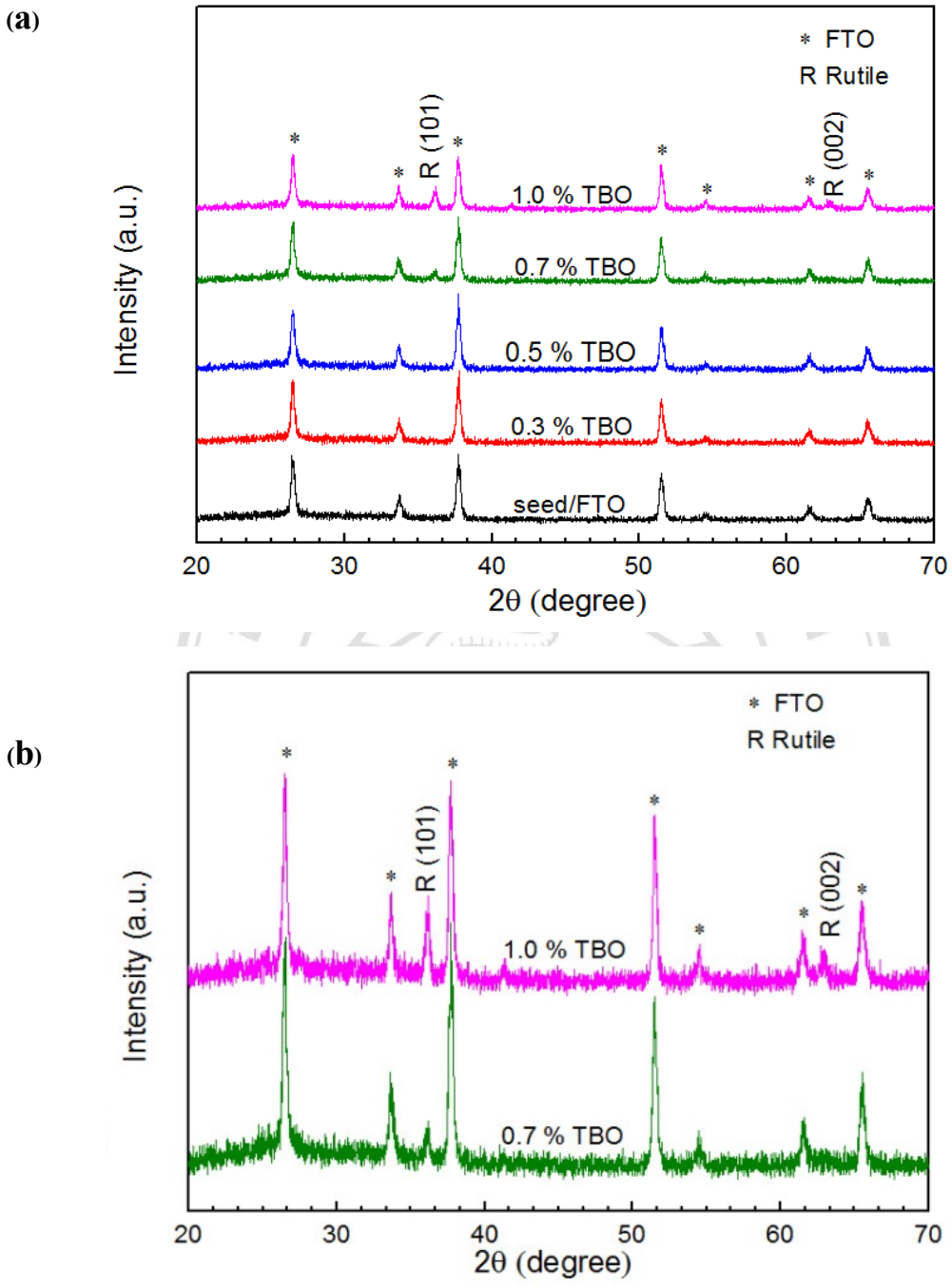


**Figure 4.9** XRD pattern of synthesized $TiO_2$ NRs on $TiO_2$ seed layer prepared on FTO substrate (a) at various TBO precursors (0.3-1.0% TBO) including $TiO_2$ seed layer and (b) at 0.7 %TBO and 1.0 %TBO

### 4.3.3 Optical Characterization by UV-VIS spectroscopy (UV-VIS)

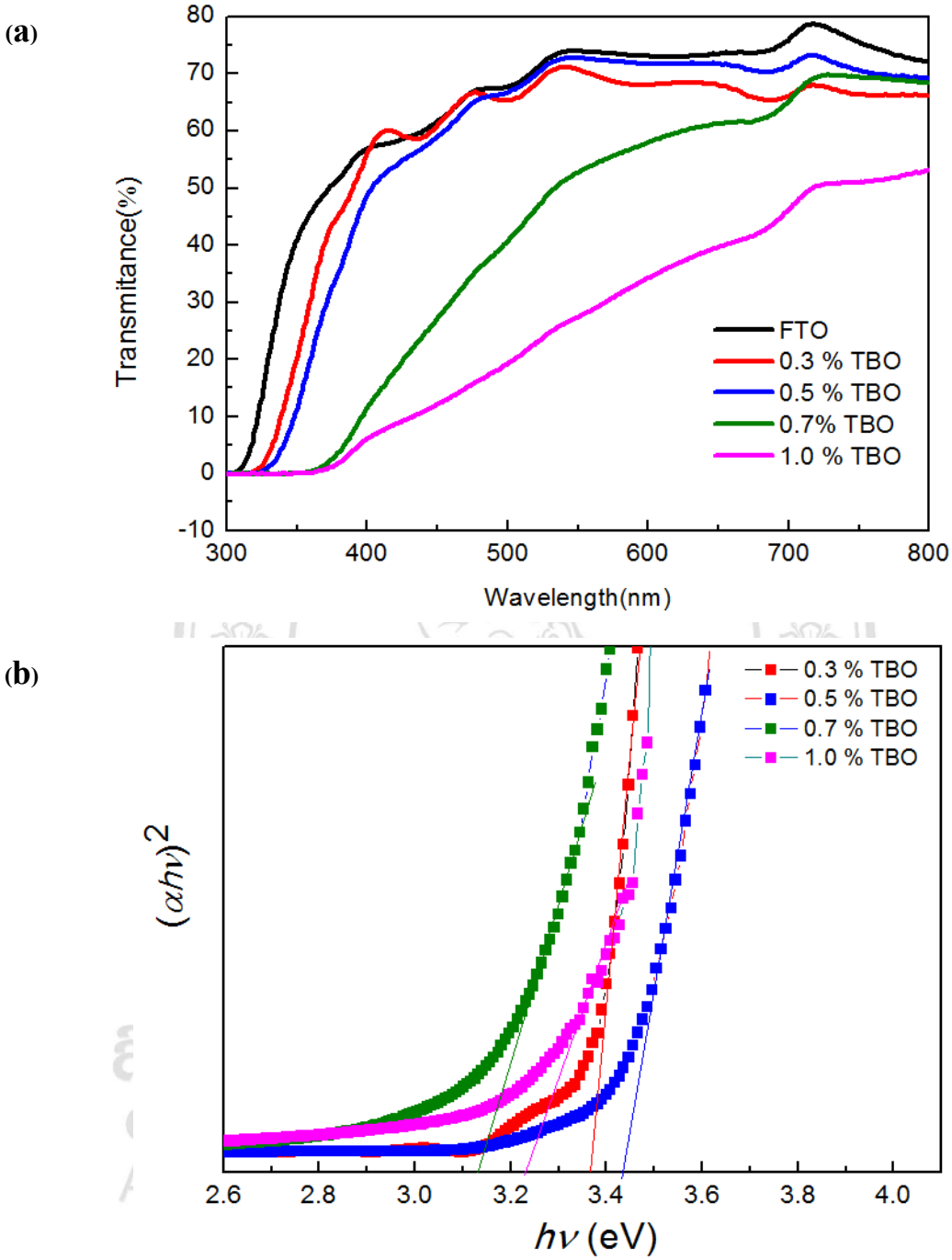


**Figure 4.10** (a) Transmittance spectra of bare FTO and $TiO_2$ NRs grown seeded-FTO substrates at different TBO concentration. (b) Relation between $(\alpha h\nu)^2$ and $h\nu$(eV) of $TiO_2$ NRs in various concentrations of TBO

Figure 4.10 (a) demonstrates transmittance spectra of bare FTO and $TiO_2$ NRs. The transmittance increased with increasing of the incident wavelength. The transmittance decreases with the increase of diameter and height of NRs, indicating that high density of vertical NRs could promote the light absorption. The 28, 103, 270 and 522 nm length NRs (0.3%, 0.5%, 0.7%, and 1.0% TBO, respectively) started to transmit light at 320, 325, 360, and 365 nm, respectively. This implies that $TiO_2$ NRs at 0.7% and 1.0% TBO could also absorb high and low light regions while that of 0.3% and 0.5% TBO NRs absorbed only high energy light.

**Table 4.2** Band gap energy of $TiO_2$ depending on phase structure and approach

| Phase | Method | Structure | Direct band gap (eV) | Indirect band gap (eV) | Ref. |
|---|---|---|---|---|---|
| Rutile | DFT | - | 1.86 | - | [28] |
| Rutile | X-ray orientation | Single crystal | 3.03 | - | [39] |
| Rutile | hydrothermal | NRs | 2.95 | - | [19] |
| Rutile | hydrothermal | NRs | 2.90 | - | [33] |
| Rutile | Reactive triode sputtering | Thin film | 3.03 | 3.05 | [40] |
| Anatase | DFT | - | - | 2.13 | [28] |
| Anatase | Commercial | Nanopowder | 3.56 | 3.25 | [41] |
| Anatase | Commercial | Bulkpowder | 3.44 | 3.21 | [41] |
| Anatase | hydrothermal | NRs | - | 3.5 | [42] |



A number of approaches has been applied to obtain band gap energies of anatase and rutile $TiO_2$ as shown in Table 4.2. Most of the researches reported that rutile is direct band gap semiconductor, however some works also report indirect band gap of rutile, either or anatase. Therefore, many studies presented both of direct and indirect band gaps. Thereby cause of assumption that rutile and anatase having both direct and indirect band gap can differ depending on fabrication and structure. For anatase, direct band gap of small particle is greater than indirect band gap, regardless of NRs. For

nanorod structure prepared by hydrothermal method, band gap of anatase phase is larger than that of rutile (about 5.05 eV) because anatase has indirect band gap which distance between valence band and conduction band is further than in (direct band gap) rutile. Due to XRD patterns of this study, it exhibits rutile phase and most of rutile has direct band gap. Thus, the $E_g$ determination of $TiO_2$ NRs was considered as the direct band gap.

The direct band gap energy $E_g$ of $TiO_2$ NRs can be obtained at 3.38, 3.43, 3.12 and 3.22 for of TBO at 0.3%, 0.5%, 0.7%, and 1.0%, respectively **(**according to Figure 4**.**10 **(**b**))**. The $E_g$ band gaps of 31-34 nm NRs (refer to 0.3% and 0.5% TBO precursor) were close to direct $E_g$ anatase and their sizes in region of stable size of anatase phase **(**< 35 nm**)** [26]. Furthermore, **(**002**)** rutile peak is in the same position as anatase (213) peak (corresponding to ICDD No. 00-002-0494 and 00-001-0562). However, previous study reported that nanorods were synthesized under 4-5 pH and 1-2 pH, resulting in an anatase and rutile phase, respectively [19]. Because in acid solution, HCl is attributed to formation of rutile structures. In dehydration reactions to form chains of Ti-octahedra, free $Cl^-$ ions take responsibility to trap migrating protons, contribute to deprotonate Ti-OH and nucleate rutile phase [21]. Thus, 31-34 nm NRs and a small (002) plane in 1.0% TBO are more likely to be rutile phase. Refer to band gap energy **(**$E_g$), in the large trend, 31-34 nm NRs had higher $E_g$. It might be low distribution of NRs and many vacancies allowed visible light piece trough the film more than 51-78 nm NRs then they were more transparent. 31-34 nm NRs exhibited high transmittance but the film dense was very low, hence absorbance were high leading to high $E_g$ (Eq 2.4-2.5). Moreover, $E_g$ of 51 nm NRs showing only (101) rutile plane was lower than that of 78 nm NRs that composted of (101) and (002). Since plane (002) has d-spacing much lower (1.47 Å) than d-spacing of (101) plane (2.22 Å), orientation of atoms in (002) plan is closer and denser. Then, electrons in close pack of atoms are bound with cation by stronger attractive force. Therefore, electrons on (002) plane require more energy to break the bound and create free electrons, leading to higher $E_g$ in 78 nm NRs.

## 4.4 Effect of hydrothermal reaction times

### 4.4.1 Characterization of morphology by field emission scanning electron (FE-SEM)

#### (a) 0.7% TBO concentration

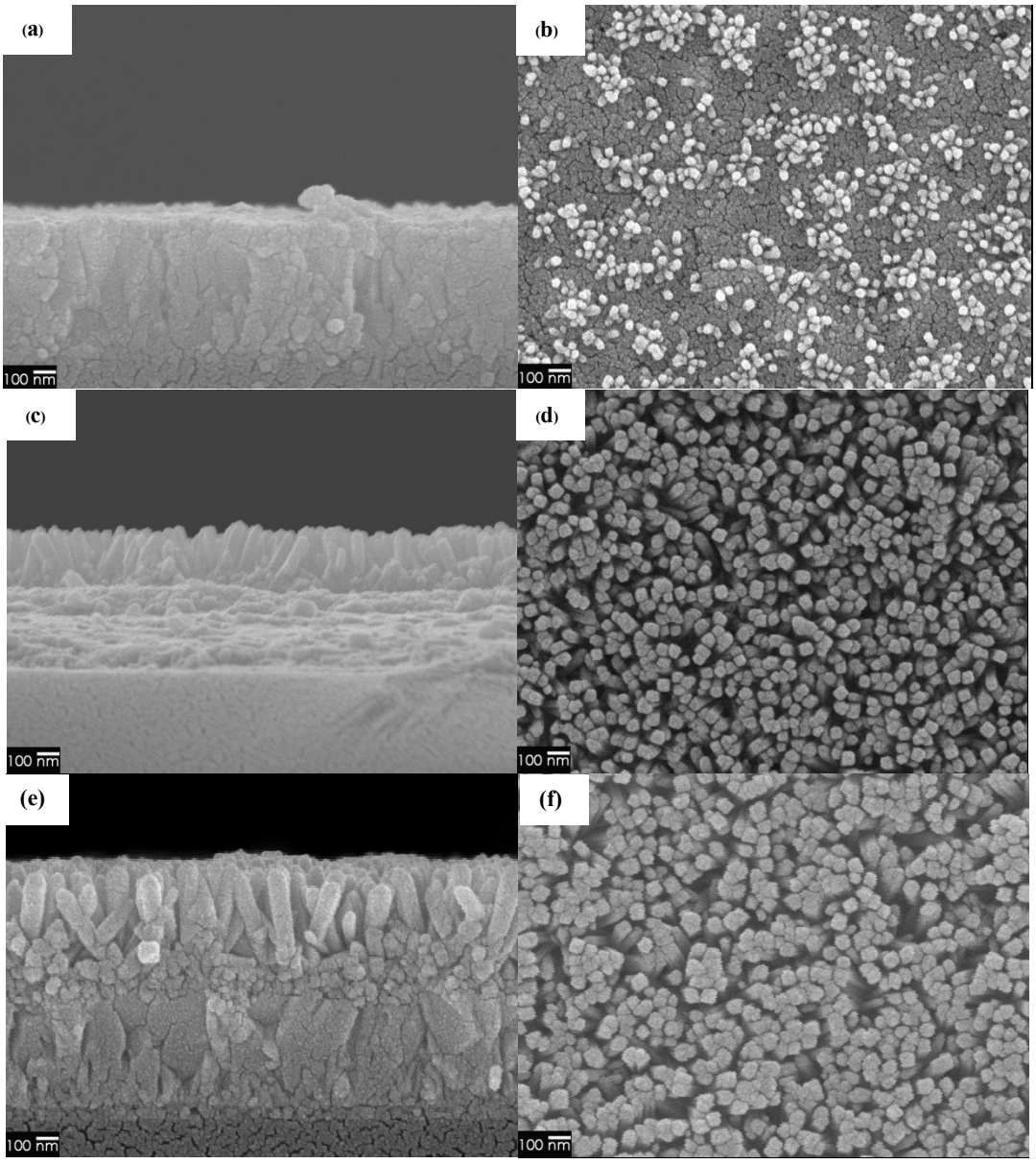


**Figure 4.11** Cross-section view and top view FE-SEM images of 0.7% TBO $TiO_2$ NRs obtained by hydrothermal reaction at (a,b) 1 h, (c,d) 1.5h and (d,f) 2 h

**(b) 1.0% TBO concentration**

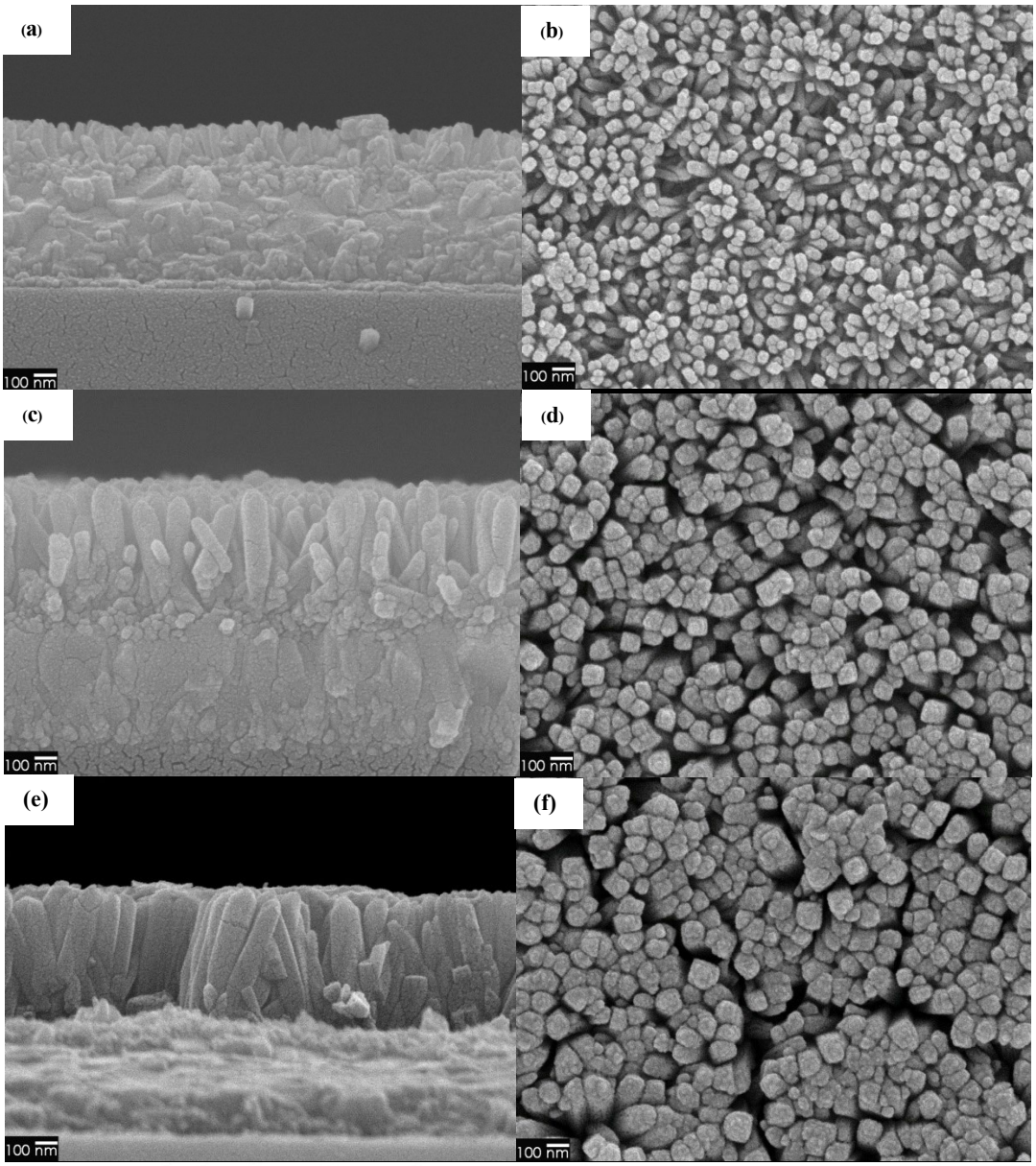




**Figure 4.12** Cross-section view and top view FE-SEM images of 1.0% TBO $TiO_2$ nanorods obtained by hydrothermal reaction at (a,b)1 h, (c,d) 1.5h and (d,f) 2 h

From Figure 4.11 and 4.12, 0.7% TBO NRs and 1.0% TBO NRs, repectively, had the same trend. Dimensions of the NRs increased with the extensive times. The average diameter and length of 0.7% TBO NRs and 1.0% TBO NRs were illustrated in Table 4.3 and 4.4, respectively. At 1.5 h of hydrothermal reaction times, length of NRs

extremely extended and moderately grew at 2 h. On the other hand, diameter had a little progress compared to the length.

**Table 4.3**.Average diameter and length of 0.7% TBO $TiO_2$ NRs at various times

| Reaction time of hydrothermal (h) | Diameter (nm) | Length (nm) |
|---|---|---|
| 1 | 39 | 56 |
| 1.5 | 51 | 270 |
| 2 | 66 | 441 |

**Table 4.4** Average diameter and length of 1.0 % TBO $TiO_2$ NRs at various times

| Reaction time of hydrothermal (h) | Diameter (nm) | Length (nm) |
|---|---|---|
| 1 | 49 | 176 |
| 1.5 | 78 | 522 |
| 2 | 96 | 614 |

Considering growth mechanism of NRs as shown in Figure 4.13, the reactions consist of 3 parts. First is hydrolysis, replacing hydroxyl groups [OH−] to bond with Ti atoms instead of alkyl groups [ R] . Second, olation is one of dehydration or condensation, which is combination of compounds to form metal oxide and release water molecule. Olation usually occurs in high acidity medium thus it is attributed to produce long chains of highly protonated Ti-complexes. Third, oxolation is another kind of condensation that is responsible in formation of greater NRs (Figure 4.13). Oxolation contributes to construct lateral arrangement in less protonated solution. During the initial reaction, since intensity of HCl is high in earliest stage, high protonation leads to fast olation. Olation takes place promptly resulting in the long chain of $TiO_6$ octrahedra with high positive charge. High amount of positive charge would obstruct further olation because the chains are not stable. $Cl^-$ ions are necessary as they contribute to deprotonate the cation with their high electronegative that strongly attract protons. During deprotonation, $Cl^-$ ions are responsible for trapping the migrating protons. This reduces the increasingly positive charge of the condensation and deprotonation and allows further reactions and removal of $OH^-$ resulting in $H_2O$ molecule. This process

called oxidation for the result of deprotonation forming $TiO_6$ octrahedra in radical direction [21]. From SEM results (Figure 4.11 (b,d,f) and Figure 4.12 (b,d,f)), growth of NRs incredibly increased in length from 1 h to 1.5 h indicating that olation occurred the most during 1 h to 1.5 h and slowed down at 2 h. As too much proton in long chain, appearing of oxolation could assist olation to continue which means diameters of NRs need to expand with length. Moreover, on account of oxolation taking place less than olation then diameters of NRs was smaller than the length.

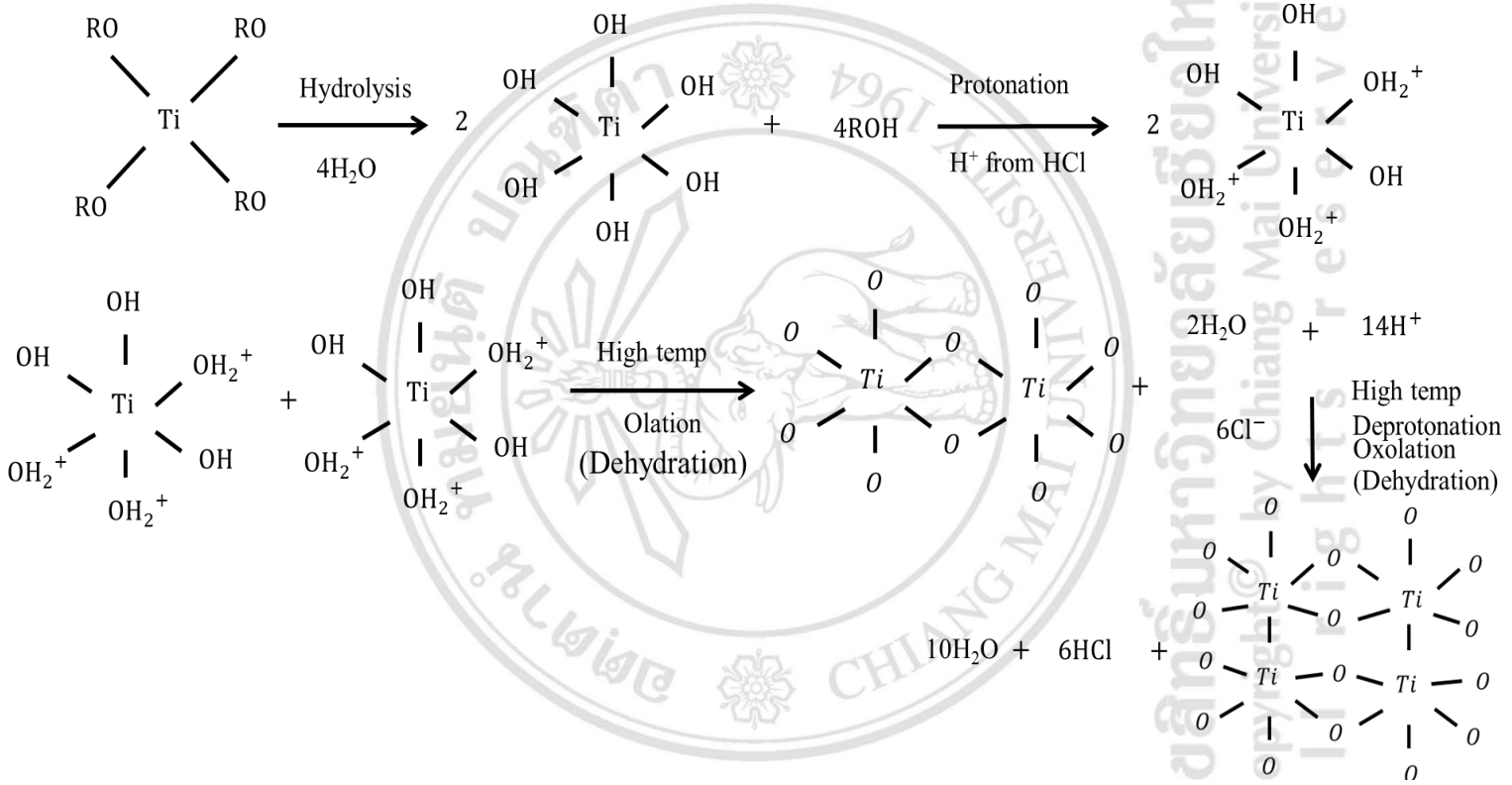


**Figure 4.13** Phase diagram of HCl role in rutile growth mechanism, where R is the component of Ti (IV)-butoxide named butyl-group with the general formula $C_4H_9$ [21, 33, 43]

### 4.4.2 Characterization of crystallinity by X-ray diffraction (XRD)

**(a) 0.7% TBO concentration**

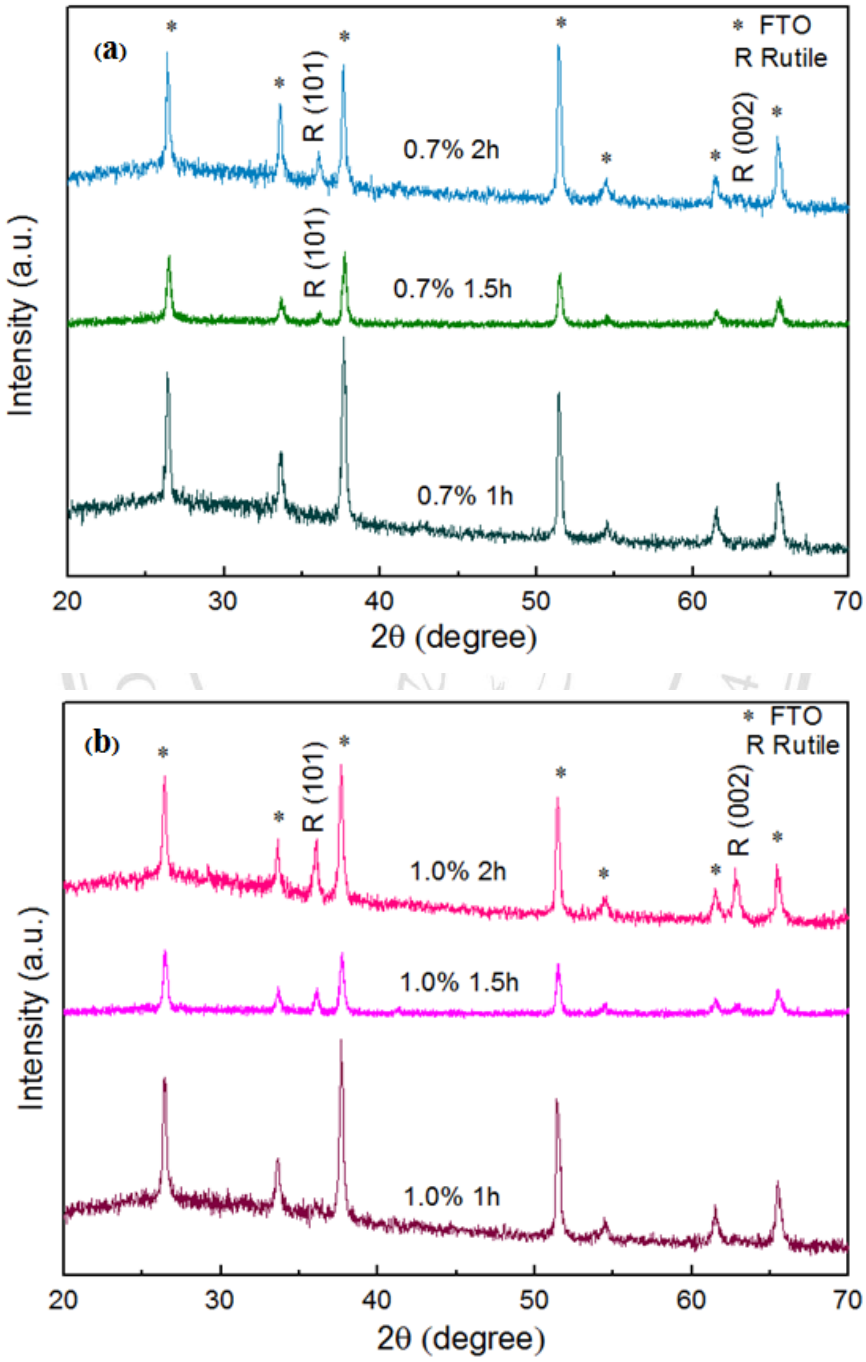


**Figure 4.14** XRD pattern of (a) 0.7% TBO $TiO_2$ NRs with reaction time 1 , 1.5, and 2 h, (b) 1.0% TBO $TiO_2$ NRs with reaction time 1 , 1.5, and 2 h

The results display that characteristic plane of (101) rutile emerges when hydrothermal method was conducted for 1.5 h with the least of for 0.7 % TBO $TiO_2$ NRs. At 1.0 %TBO $TiO_2$ NRs, there were (101) plane of rutile and a small (002) rutile peak as present in 0.7 % TBO $TiO_2$ NRs when the reaction duration reached to 2 h. When hydrothermal process was prolonged to 2 h for 1.0 % TBO $TiO_2$ NRs, the intensity of (002) peak was higher than that at 1.5 h. Moreover, it was obvious that (101) plane emerges before (002) plane because (101) is one of the lowest energy plane, that is easier to be initiated [21]. When the hydrothermal reaction was conducted for 4 h the (002) intensity increases dramatically that demonstrates the dominant plane of NRs growth on SLs was (002) rutile corresponding to previous study [19,36].

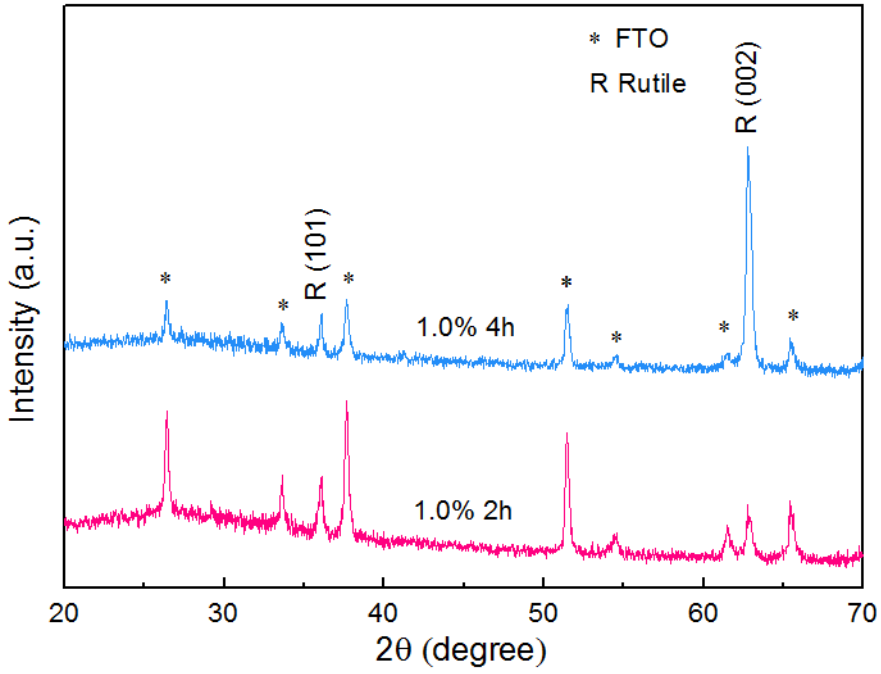


**Figure 4.15** XRD pattern of 0.7% TBO $TiO_2$ NRs with reaction time 2 h and 4 h

### 4.4.3 Structural characterization by transmission electron microscope (TEM)

Selected area electron diffraction patterns (SAED) (Figure 4.16 (c) and Figure 4.17 (e,f)) show that 0.7% TBO NRs and 1.0% TBO NRs have single crystalline structure. While (002) plane is dominated for the large NRs with high crystallinity (from Figure 4.15). The single-crystal architecture is significant to apply in solar cell,

because NRs offer fast pathway via the length with less grain boundary. In addition, fewer defect traps present in single crystal NRs compared to poor crystalline leading to lower recombination [44]. Figure 4.16 (b) represents HRTEM of 0.7% TBO NRs consisting of (110) growth along [100] direction with d-spacing 2.92 Å confirm with SAED of 0.7% TBO NRs (Figure 4.16 (c)) which is the evidence of (110) plane orientation within the NRs. For 1.0% TBO NRs, Figure 4.17(b) displays orientation of (110) face of the NRs observed at "a" area of Figure 4.17(a). From investigation of "b" area of 1.0% TBO NRs (Figure 4.17(d)), lattice fringes of (101) and (002) facets were found as present in Figure 4.17(f). The (101) plane shows interplanar spacing 2.24 Å while (002) face exhibits a great lower d-spacing with 1.47 Å. This is the reason why (002) is the prominent plane. This corresponded with XRD result that (101) and (002) rutile peak could be detected in hydrothermal of 1.0% TBO NRs for 1.5 h.

In order to investigate the fundamental understanding behind the growth mechanism, explanation of related planes of rutile structure will be considered. Dominant planes of tetragonal rutile $TiO_2$ structure in this work consist of (110), (101) and (002). Atoms arrangements of these faces in three dimension and side views are demonstrated in Figure 4.18. For clearly illustration of the planes orientation in crystal, Figure 4.19 shows alignment of $TiO_6$ octahedra into planes and growth direction of each facet. It can be seen that (110) orientation in Figure 4.19 (b) correspond to (110) bright spot in Figure 4.16 (c,e) and Figure 4.17 (f) representing the lattice fringes matching with (101) and (002) faces in Figure 4.19 (d,f).

In aspect to describe crystal growth phenomena, surface energy is relative. Surface energy is determined as the surface excess free energy per unit area of a specific. It determines the equilibrium shape of crystals and crystal development [45]. Generally, internal attraction between bulks is balance but at the interfacial area attraction energy is unstable. Therefore, facial atoms form themselves into films at the surface resisting external force. Further crystallization to form new surface requires surface energy in order to break the intermolecular force of the surface [46]. The energy depends on amount of atoms at surface, thus surface energy is upon direction. Recently, several approaches have been performed to clarify surface energy of rutile $TiO_2$. On the base of previous report, (110) rutile was found as the lowest surface energy face with the most stability [47]. In this work, (110) which could not be detected by XRD but

was observed by SAED mode of TEM because (110) oreints in direction that does not promote constructive interferrance resulting in diffraction in unsuitable direction to match with the detector.

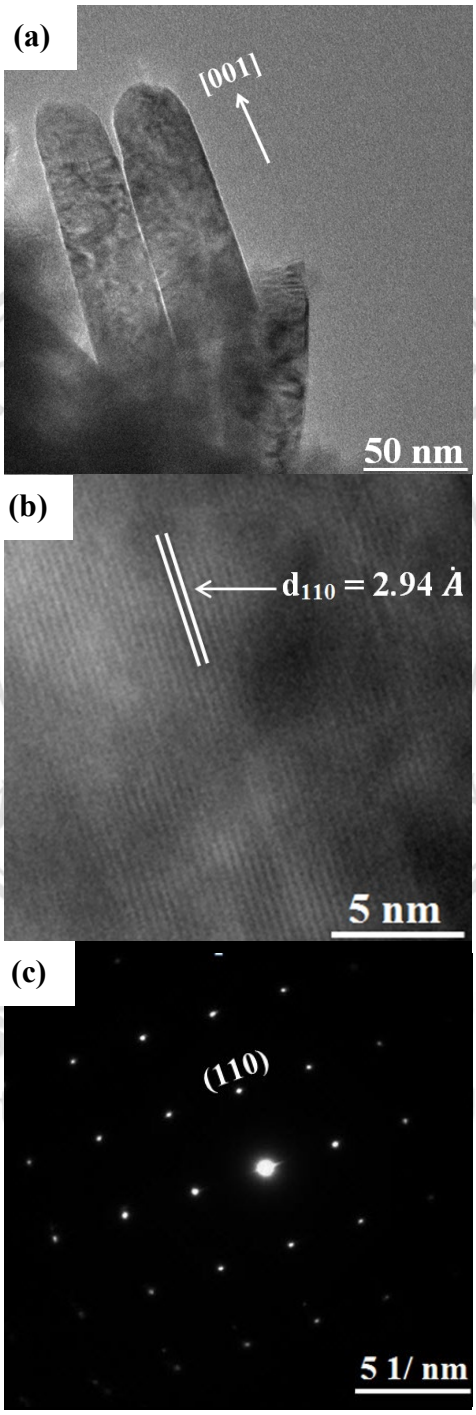


**Figure 4.16** Image of 0.7% TBO $TiO_2$ NRs hydrothermal for 1.5 h (a) TEM (b) high resolution transmission electron microscope (HRTEM) of Figure (a) (c) Selected area electron diffraction patterns (SAED) of (110) plane

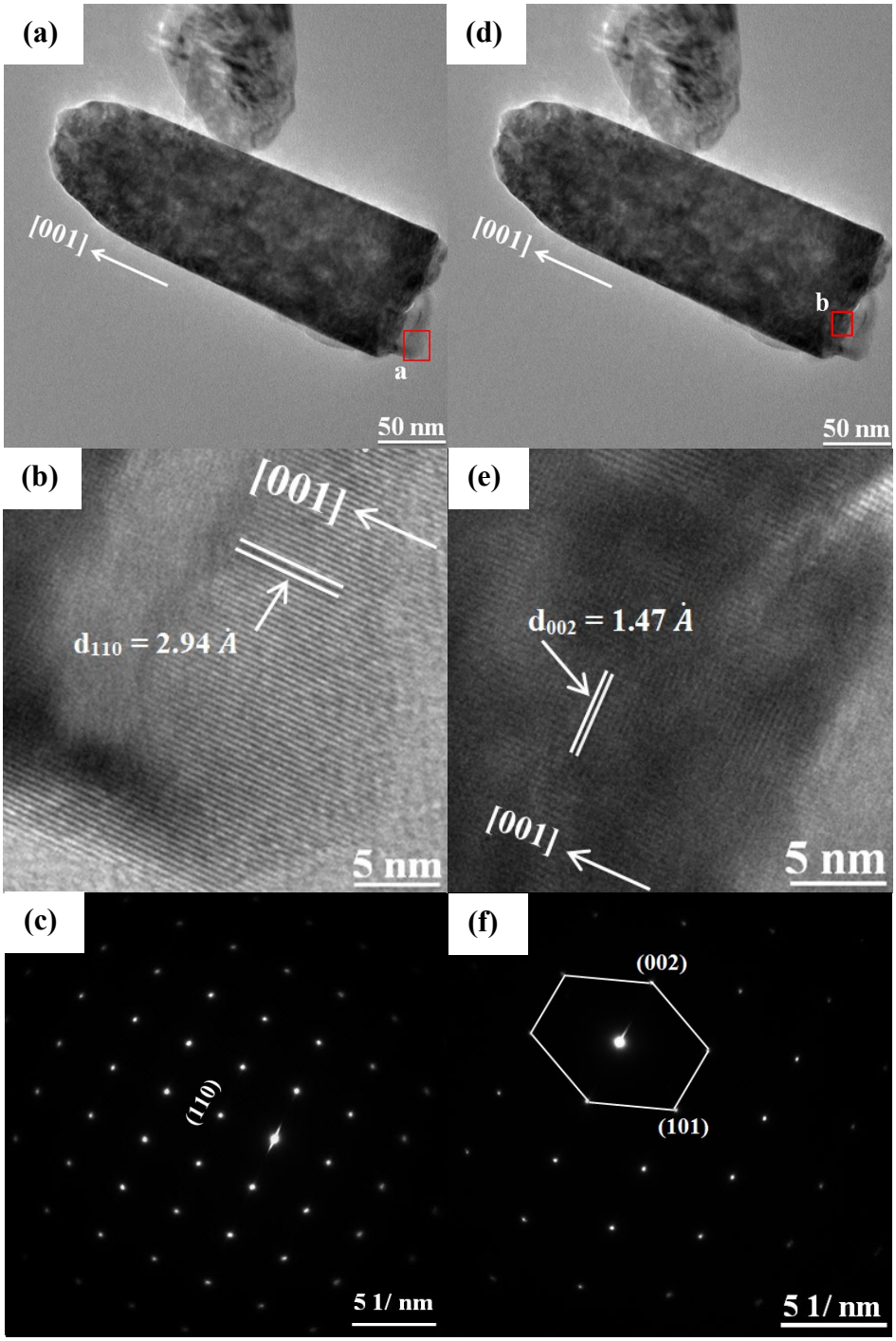


**Figure 4.17** Image of 1.5 h hydrothermal of 1.0% TBO $TiO_2$ NRs (a,d) TEM (b) high resolution transmission electron microscope (HRTEM) of "a" area (c) selected area electron diffraction patterns (SAED) of "a" areas (e) HRTEM of "b" area (f) SAED of "b" area

According to XRD and TEM outcomes, it is obvious that (101) plane firstly took place followed by formation of (002) plane when the hydrothermal reaction time increased. This effect can be explained by geomatrical configuration of (101) and (002) surface. Because (101) surface possessed fivefold coordinated titanium atoms (petacoordinated; Ti(5)) while (002) facet composed of fourfold coordinated titanium atoms (Ti(4)), (002) plane required more energy to continue their growth into $TiO_6$ octahedra relative to (101). In other words, (002) face had higher energy surface than (101) face [47, 48]. Moerover, there are more uncomplete Ti(5) on (101) plane than (110) one, then (110) surface demanded few amount of energy and less molecules of Ti-complex to bond with and completeed its development into new plane. Thereby, surface energy of (101) (1.85 $J/m^2$) is more than that in (110) (1.78 $J/m^2$) [47,49]. When the hydrothemal was proceeded for 4 h, (002) became intense. While (101) stopped growing supporting form XRD data in Figure 4.15. Geomatrical reasons migh be used to revealed mechanism of this phenomena. Because (101) orients againts [001] direction with an angle as shown in Figure 4.18 (c) and Fgure 4.19 (c,d), development (101) results in incresing of NRs in width and lenhth but the specific area is restriction of growing in latheral. When the diameter of NRs grew and their walls contacted with the neighboring NRs, (101) plane could no loger extent. On the other hands, (002) with its small d-spacing aligns perpendicular to (Figure 4.18 (f) [001] direction and the preferential growth rutile NRs is [001] direction. Number of (002) plane will increase with the length of NRs and does not restrict by latheral area. Therefore, the extreme growth of NRs in [001] direction results in a gtreat number of (002) face. This is the reason why (002) plane is dominate. Morevor, an enhancement of $TiO_6$ octahedra on the surface could restrict further oxolation of $[TiO(OH_2)_5]^{2+}$ complex on (101) surface [33]. Another approach referred that HCl play a role to reduce the surface energy of the crystal plane side wall, supporting anisotropic growth in the [001] direction [50].

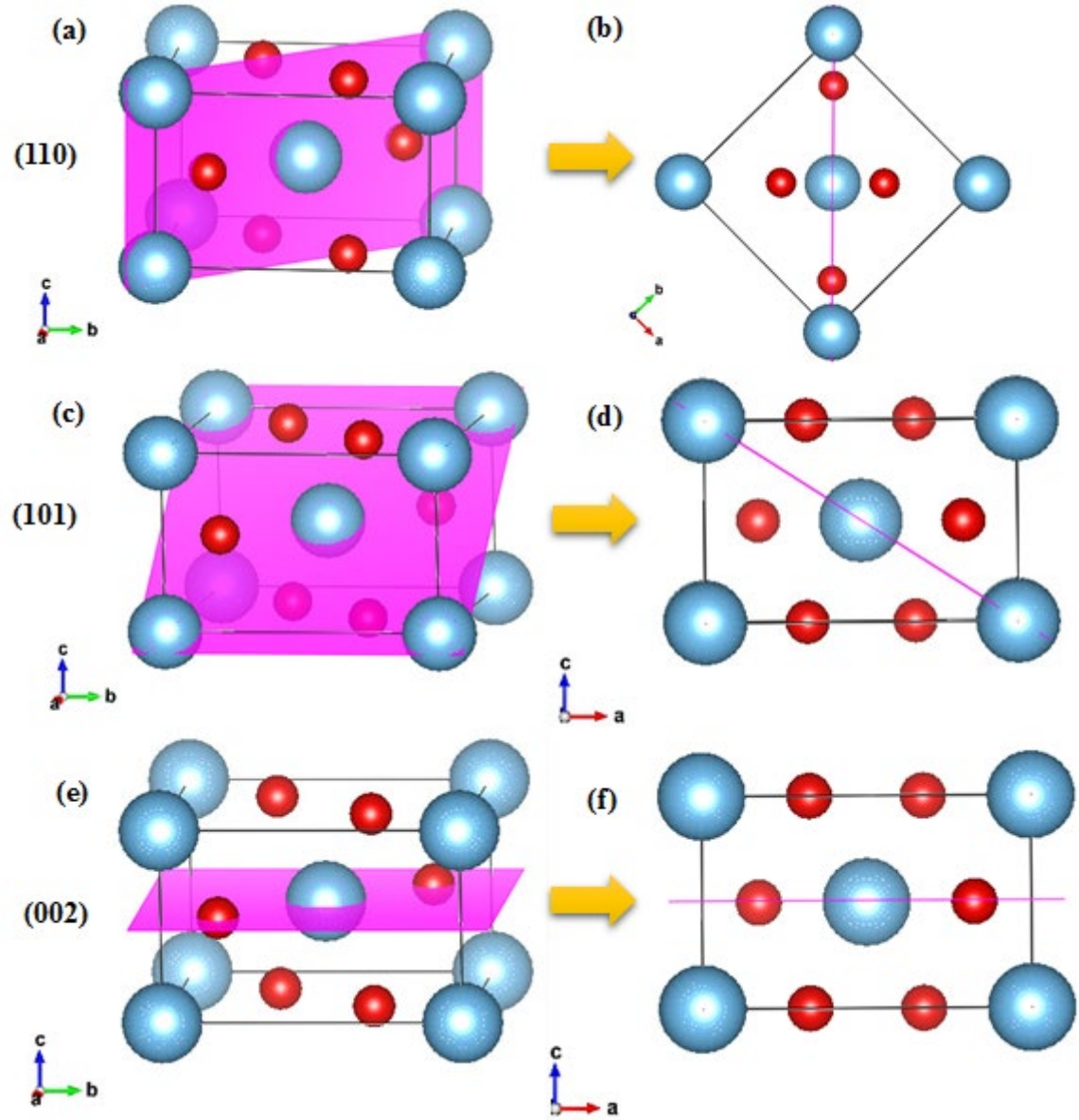


**Figure 4.18** Dominant planes of rutile $TiO_2$ structure; (a) (110) plane in 3D space, (b) (110) plane in [001] direction, (c) (101) plane in 3D space, (d) (101) plane in [010] direction, (e) (002) plane in 3D space and (f) (002) plane in [010] direction [49].

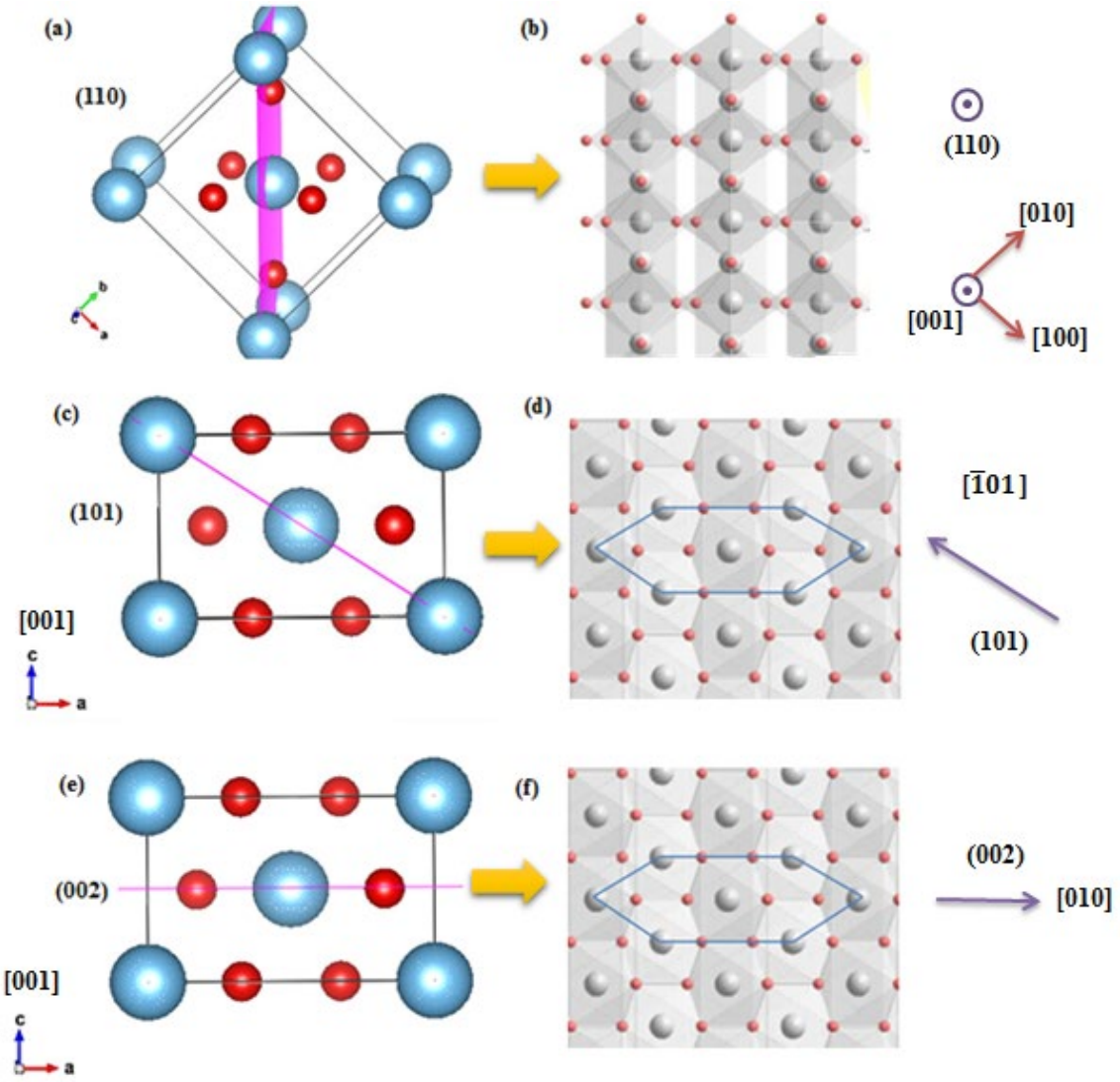


**Figure 4.19** Dominant planes of rutile $TiO_2$ structure; (a) (110) plane in $[1\bar{1}0]$ direction (b), orientation of (110) plane, (c) (101) plane in [010] direction (d) orientation of (101) plane, (e) (002) plane in [010] direction and (f) orientation of (002) plane